Compton Scattering on ^{6}Li with Nuclear One- and Two-Body Densities

24th February 2025

Alexander P. Long[a], **Harald W. Grießhammer**[abc] [1], **Xiang-Xiang Sun**[d]
Andreas Nogga[d2]

[a] *Institute for Nuclear Studies, Department of Physics, The George Washington University, Washington DC 20052, USA*

[b] *Department of Physics, Duke University, Box 90305, Durham NC 27708, USA*

[c] *High Intensity Gamma-Ray Source, Triangle Universities Nuclear Laboratories, Box 90308, Durham NC 27708, USA*

[d] *IAS-4, IKP-3 and JCHP, Forschungszentrum Jülich, D-52428 Jülich, Germany*

Abstract

We present the first *ab initio* calculation of elastic Compton scattering from ^{6}Li. It is carried out to $\mathcal{O}(e^2\delta^3)$ in the δ expansion of χEFT . We assess the sensitivity of the cross-section to bean asymmetry and nucleon polarisabilities.

Suggested Keywords: Chiral Effective Field Theory, proton, neutron and nucleon polarisabilities, ^{6}Li Compton scattering, $\Delta(1232)$ resonance, pion-exchange currents, Transition Density Method

[1]Email: hgrie@gwu.edu; permanent address: *a*
[2]Email: a.nogga@fz-juelich.de

1 Introduction

Elastic Compton scattering on light nuclei with energy high enough to probe the internal structure of the nuclei without getting into the resonance structure allows us to quantify two important effects. First, it allows us to determine the neutron electric and magnetic scalar dipole polarisabilities (α_{E1} and β_{M1} respectively). These parameters measure stiffness against deformation of a nucleus, and enter the nucleus Hamiltonian in the form

$$\mathcal{H} = -4\pi \left(\frac{1}{2}\alpha_{E1}\vec{E}^{\,2} + \frac{1}{2}\beta_{M1}\vec{H}^{\,2} \right) \tag{1.1}$$

Therefore, they can be inferred in Compton scattering data. Second, Compton scattering in this regime shows the impact of the two-body, pion mediated currents. *One more sentence on why this is important* . Compton scattering experiments on protons and light nuclei have been a subject of much interest over the past 25 years. In particular, experimental results exist for ^{6}Li Compton scattering at 60MeV [42] and 86MeV [43]. Chiral Effect Field Theory (χEFT) is used to interpret this data, as well as provide systematic uncertainty estimates. χEFTprovides a model independent approach which organizes interactions via a small expansion parameter which in turn provides a hierarchy of scales. This order by order approach allows for the determination of the uncertainty associated with the calculation due to truncation of terms.

To date the best estimates for neutron polarisabilty result from Compton scattering on the deuteron [40, 39, 38]. The isospin averaged polarisabilities are

$$\alpha_{E1}^{(s)} = 11.1 \pm 0.6_{\rm stat} \pm 0.2_{\rm BSR} \pm 0.8_{\rm th} \;\;,\;\; \beta_{M1}^{(s)} = 3.4 \mp 0.6_{\rm stat} \pm 0.2_{\rm BSR} \pm 0.8_{\rm th} \tag{1.2}$$

where we have used (and will continue to use) the canonical units of 10^{-4}fm^3. Note BSR (Baldwin Sum Rule) is used here: $\alpha_{E1}^{(s)} + \beta_{M1}^{(s)} = 14.5 \pm 0.4$. The uncertainty here comes from omitted higher order terms in the χEFT expansion. The proton polarisabilities can be determined directly:

$$\alpha_{E1}^{(p)} = 10.65 \pm 0.35_{\rm stat} \pm 0.2_{\rm Baldin} \pm 0.3_{\rm th} \;\;,\;\; \beta_{M1}^{(p)} = 3.15 \mp 0.35_{\rm stat} \pm 0.2_{\rm Baldin} \mp 0.3_{\rm th} \;\;. \tag{1.3}$$

and as a result the proton-neutron polarisabilty difference has an uncertainty larger than the measurement itself

$$\alpha_{E1}^{(p)} - \alpha_{E1}^{(n)} = [-0.9 \pm 1.6_{\rm tot}]\,. \tag{1.4}$$

Further description and motivation for interest in the polarisabilities can be found in Greiβhammer et. al 2024 [41].

In this work we extend the analysis of Compton scattering on ^{3}He and ^{4}He to ^{6}Li [41, 44]. This is the first time a six body system has been analyzed with the transition

density method, and novel techniques were required to deal with the increased size of the phase space. In particular a similarity renormalization group (SRG) transformation has been used along with a corresponding back transformation to physical momenta.

2 Formalism

2.1 The Transition Density Method

We use the *Transition Density Method* as described in detail in refs. [41, 44, 37]. This method factors the interaction into a part describing only the reaction, for example Compton scattering, and are part describing only the target, for example ^{6}Li. Consider a probe γ scattering off an arbitrary nucleus X with A nucleons; then the reaction is $\gamma X \to \gamma X$, and the probe my interact with any number of nucleons $n = 1, 2..., A$. Fortunately χEFT provides a hierarchy of scales which predicts the contributions to the matrix element go as $\mathcal{O}(Q^n)$ so the many body interactions are suppressed at these energies. In practice we consider only $n = 1$ and $n = 2$, which correspond to one- and two-body densities respectively. In this approach n nuclei are then *active*, leaving the remaining $A - n$ nuclei as *spectators*. The total scattering amplitude is given by:

$$\begin{aligned} A^{M'\lambda'}_{M,\lambda}(\vec{k},\vec{q}) &= \binom{A}{1} \langle M'| \hat{O}_1^{\lambda,\lambda'}(\vec{k},\vec{q}) |M\rangle + \binom{A}{2} \langle M'| \hat{O}_2^{\lambda,\lambda'}(\vec{k},\vec{q}) |M\rangle \\ &+ \binom{A}{3} \langle M'| \hat{O}_3^{\lambda,\lambda'}(\vec{k},\vec{q}) |M\rangle + \binom{A}{4} \langle M'| \hat{O}_4^{\lambda,\lambda'}(\vec{k},\vec{q}) |M\rangle + ... \qquad (2.1) \\ &= \binom{A}{1} \langle M'| \hat{O}_1^{\lambda,\lambda'}(\vec{k},\vec{q}) |M\rangle + \binom{A}{2} \langle M'| \hat{O}_2^{\lambda,\lambda'}(\vec{k},\vec{q}) |M\rangle + \mathcal{O}(Q^3) \qquad (2.2) \end{aligned}$$

Here $\hat{O}_n$ represents the n-body kernel, and the symmetry factors arise from there being $\binom{A}{n}$ ways for a probe to interact with n nuclei out of A total options. Here λ, λ' are the initial and final states of the probe, which in the case of Compton scattering happens to be the polarisations. We now introduce the n-body transition density ρ_n, which is dependent on all the quantum numbers of the nucleus along with the relevant momenta. We shall immediately drop the subscript n on ρ_n as it is always obvious by context which density is being discussed. Then up to relativistic corrections we can write the one-body contribution as:

$$\left\langle M' \left| \hat{O}_1(\vec{k},\vec{q}) \right| M \right\rangle = \sum_{\substack{m_3^{s\prime} m_3^s \\ m_3^t}} O_3\left(m_3^{s\prime} m_3^s, m_3^t; \vec{k}, \vec{q}\right) \rho^{m_3^t M_T, M'M}_{m_3^{s\prime} m_3^s}(\vec{k},\vec{q}) \,. \qquad (2.3)$$

And similarly for the two-body interaction

$$\left\langle M' \left| \hat{O}_2 \right| M \right\rangle = \sum_{\alpha'_{11},\alpha_{12}} \int \mathrm{d}p_{12}\, p_{12}^2\, \mathrm{d}p'_{12}\, p'^2_{12}\, O_2^{\alpha'_{12}\alpha_{12}}(p'_{12}, p_{12})\, \rho^{M_T,M'M}_{\alpha'_{12}\alpha_{12}}(p'_{12}, p_{12}; \vec{q}) \,. \qquad (2.4)$$

Where α parameterizes all the quantum numbers of the system,

$$|\alpha\rangle = |[(l_{12}s_{12})\, j_{12}\, (l_3 s_3)\, j_3]\, JM, (t_{12}t_3)\, TM_T\rangle\,. \tag{2.5}$$

The two-body case is similar to the one-body case except now one must integrate over the free momenta. The reader is encouraged to see ref.[44] for a complete derivation.

We emphasize that the work presented here focuses on the Compton scattering kernel development, that is the implementation of O_1 and O_2. The work on the densities is separate, and software that calculates Compton scattering in this framework takes the densities as an external parameter. The immediate advantage here is that new kernel interactions can be developed, and can then immediately use the pre-existing densities.

3 SRG Transformation

Previous work using the TDA formalism has analyzed ^{3}He and ^{4}He [44, 41] , but to extend this to ^{6}Li involves many-body interactions which are much more complicated and computationally expensive. To make the calculation of a TDA feasible for $A = 6$, a *similarity renormalization group* (SRG) transformation is employed [45, 46]. This is of much experimental interest since ^{6}Li is a stable solid at room temperature and is therefore relatively simple to conduct an experiment on, even to high precision due to its relatively large cross section and count rate. There have been many experiments on ^{6}Li [42, 43], yet to date there is no theory prediction, we seek to fill in this gap. When using nuclear potentials, we approximate the nucleon-nucleon potential to be zero beyond a certain cutoff Λ_{NN}, and consequently neglect contributions above this cutoff in our calculations. In general, a nuclear potential, such as the chiral SMS potential does not fall off rapidly at high momenta [48]. As a result we would have to extend the cutoff Λ_{NN} much further than is desirable, which in turn increases computational cost. The SRG transformation is a unitary transformation that shifts the relevant physics into the low-momentum region, thereby lowering minimum effective Λ_{NN} in the SRG evolved space. This, in turn, significantly improves the convergence rate of calculations for $A = 6$. The SRG transformation can be thought of as a local averaging or smoothing of the potential, resulting in decreased resolution has the SRG is applied.

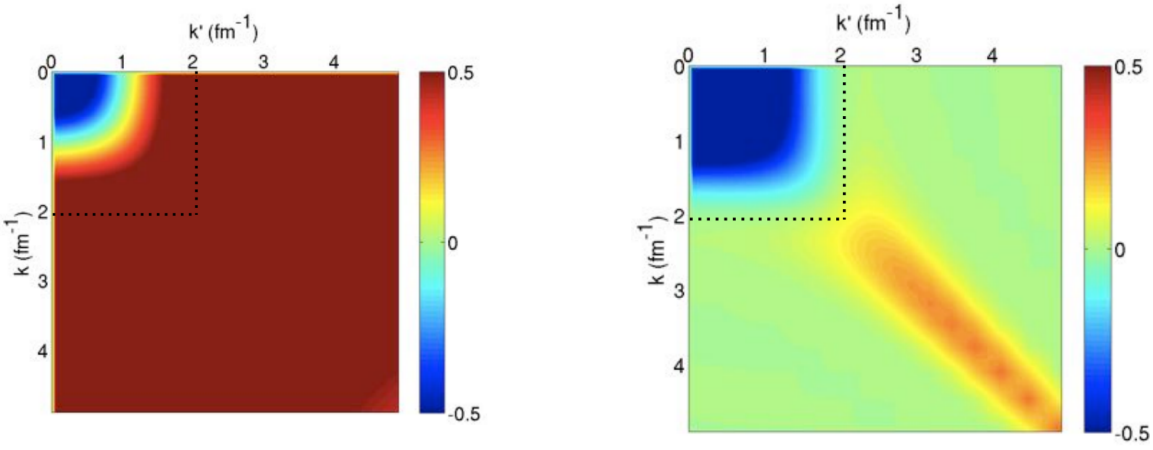

(a) High Resolution, before much SRG is applied

(b) Low Resolution after lots of SRG is applied

Figure 1: Nuclear potentials $V(k, k')$. Figures from Kai Hebeler: "Chiral Effective Field Theory and Nuclear Forces: overview and applications" presentation at TALENT school at MITP 2022, and modified with permission from Furnstahl *et al.*[46].

In the under-evolved, high resolution figure 1a the potential does not go to zero rapidly, whereas it does once the transformation is applied in figure 1b. As a result a cutoff can be made at $\Lambda_{\mathrm{NN}} = 2\mathrm{fm}^{-1}$ without losing much accuracy whereas the under-evolved potential required at least $\Lambda_{\mathrm{NN}} = 5\mathrm{fm}^{-1}$. The time complexity is at minimum proportional to the number of array elements present, therefore we gain a factor of $(5/2)^2 = 6.25$ in efficiency; in practice the gains are even higher.

The SRG transformation is essential, but it also creates a change in the physical meaning of the free variables. In fact, any unitary transformation ($U^\dagger U = \mathbb{1}$) also transforms the coordinates.

$$\langle p'|\, V\, |p\rangle = \langle p'|\, U^\dagger U V U^\dagger U\, |p\rangle = \langle p'|\, U^\dagger \left(UVU^\dagger\right)\, U\, |p\rangle = \langle \widetilde{p}\,'|\, V_{eff}\, |\widetilde{p}\rangle = V_{eff}(\widetilde{p}, \widetilde{p}\,') \tag{3.1}$$

So referring to the free variables in an SRG-transformed potential as "momenta" is, to some extent, incorrect. They do not represent physical states in the sense that they are not eigenstates to physical momenta. The Lagrangeans that generate the Feynman diagrams in the kernel, however, depend on physical momenta, and therefore we cannot directly use an SRG evolved potential in the non-SRG evolved kernel. To solve this, previous work with SRG transformations has transformed the Lagrangeans - and therefore the kernels - into the SRG evolved space as well *get citation* . However, in the context of the density formalism this would mean adding SRG dependence into the kernel, thereby breaking kernel-density independence. Additionally, the SRG transformation can take many different forms [45, 46]; we wish to allow for these developments without having to re-write the kernel code. Therefore we have chosen to apply an inverse transformation to the densities [47].

The SRG evolution has parameters that must be fine-tuned, but this allows for uncertainty estimation. In particular, one must solve for the nucleus wavefunction; to this end an expansion in the harmonic oscillator basis is used. When expanded to infinite order, this basis forms a complete set, however, we truncate this expansion by including harmonic oscillator excitations up to N_{tot}. Additionally, the harmonic oscillator basis has a characteristic width, denoted by ω_H, and finally, the parameter Λ_{SRG} represents the evolution of the potential, as seen in figure 1. $\Lambda_{\text{SRG}} = \infty$ corresponds to no evolution. All of these parameters affect the resulting cross-section. We note that uncertainty decreases monotonically with increasing N_{tot}, and at $N_{\text{tot}} = \infty$ the associated uncertainty goes to zero. Applying a stronger SRG evolution (lower Λ_{SRG}) to the potential results in larger induced many-body forces; however, we show in figure 2 the effect of this uncertainty is small. These induced forces exist because due to the cutoff Λ_{NN} the SRG transformation is only approximately unitary. Fortunately, when the TDA is calculated we also gain access to the binding energy of the simulated system. From this, we can estimate required values for ω_H and N_{tot} by comparing the experimental binding energy to computed binding energy. In order to gain confidence we first applied this methodology to ^{4}He, where we can compare SRG and non-SRG evolved results. With this completed we have now moved to ^{6}Li where we only have access to the SRG evolved form.

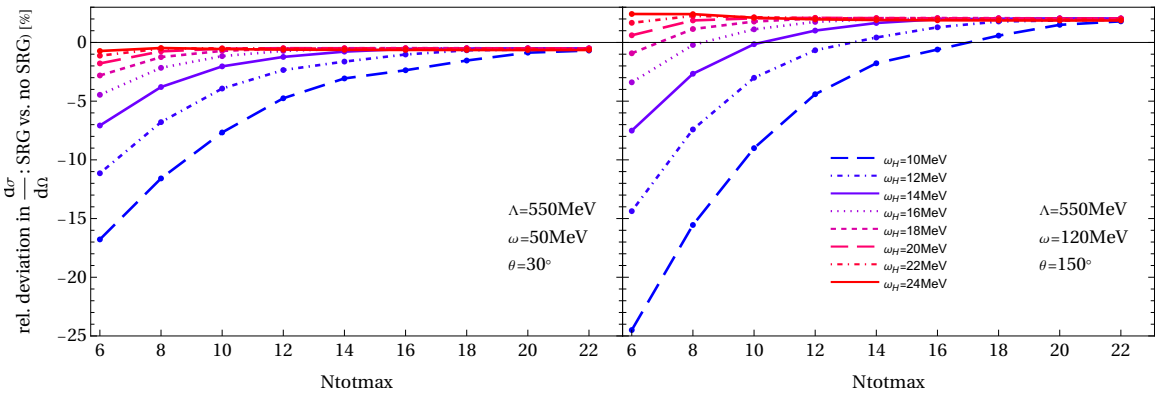

Figure 2: ^{4}He Compton scattering SRG convergence

$$\text{“Relative deviation, (Rel. deviation) of } A \text{ from } M\text{”} := \frac{A}{M} - 1 \tag{3.2}$$

In figure 2, we see the effectiveness of the results in the ^{4}He case. We expect the deviation to decrease as N increases, and importantly for our analysis, this shows what value of N is required. The small error present at high N_{tot} is present do to the induced many body forces.

To estimate the uncertainty associated with the N_{tot} expansion, we utilize the form of plots as a function of N_{tot} and ω_H.

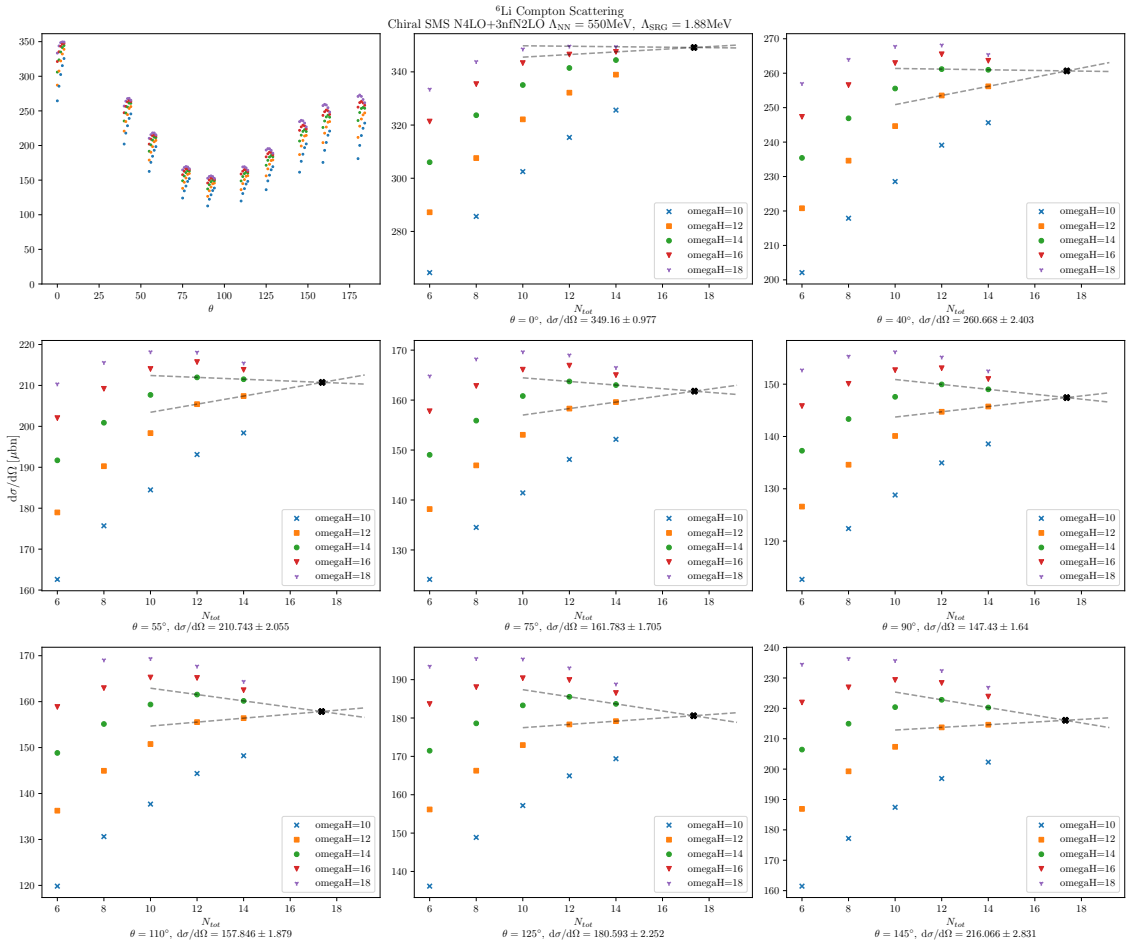

Figure 3: Compton scattering on ^{6}Li,

First note that these values appear to be converging either from above or below depending on the value of ω_H To this end we use the squeeze theorem which grantees convergence in that range. Considering first the values of ω_H which reproduce the binding energy most accurately ($\omega_H = 14, 16$), we check if we have one instance that is converging from above, and one from below. If we do not, then we check the next available values of ω_H. For the chosen values of ω_H let $(x, y)_{1,a}$, $(x, y)_{2,a}$ be the coordinates on the points with the negative slope and let $(x, y)_{1,b}, (x, y)_{2,b}$ be the values of the points associated with the negative slope. Here the x values are N_{tot} and the y values are the cross section. That is, a represents one value of ω_H and b another, also let $x_1 < x_2$. The reported central value comes from the intersection of the lines that interpolate the a and b points respectively. The reported uncertainty is $\sigma_{N_{tot}} = |y_{2a} - y_{2b}|/2$. Note this is only the uncertainty associated with this procedure, other forms of uncertainty contribute.

3.1 Compton Scattering Observables in Lithium Six

The momentum transfer $\vec{q}$ describes the transition densities, and can be replaced by the energy of the incoming and outgoing photon along with the scattering angle θ_{cm}. We have $\omega_{\text{cm}} = |\vec{k}| = |\vec{k}'|$, and

$$\cos\theta_{\text{cm}} = 1 - \frac{\vec{q}^2}{2\omega_{cm}^2} \tag{3.3}$$

The ^{6}Li Compton cross section (with target spin $0 = M = M'$) in the lab frame is found by transferring the energies and angles from the center of mass from using the ^{6}Li mass of 5603.1 MeV.

$$\frac{\mathrm{d}\sigma}{\mathrm{d}\Omega} = \frac{1}{6}\left(\frac{\omega'_{\text{lab}}}{4\pi\omega_{\text{lab}}}\right)^2 \sum_{\substack{M,M'\\ \lambda\,\lambda'}} \left|A_{M\lambda}^{M'\lambda'}(\vec{k},\vec{q})\right|^2 \quad . \tag{3.4}$$

Where the average over the spins and the polarizations give the prefactor $\frac{1}{6} = \frac{1}{2}\cdot\frac{1}{3}$ (Why is is not $\frac{1}{2+3}$)

I can't find a definition of ω_{lab} and ω'_{lab}.

There is one more equation about asymmetry (2.8) in the ^{4}He paper, but this sounds like it could be spin dependent, I will leave it out for now.

3.2 Compton Kernel

This is word for word from the ^{4}He paper

For reviews of Compton scattering on nucleons and light nuclei in χEFT , we refer the reader to refs. [36, 35] for notation, relevant parts of the chiral Lagrangian, and full references to the literature. Here, we merely summarise the power counting and Compton kernel already employed in refs. [33, 32, 34] in our region of interest, 50 MeV $\lesssim \omega \lesssim$ 120 MeV.

When χEFT with a dynamical Delta is used to compute (elastic) Compton scattering, three low scales compete: the pion mass m_π, the Delta-nucleon mass splitting $\Delta_M \approx 300$ MeV, and the photon energy ω. Each provides a small, dimensionless expansion parameter, measured in units of the "high" momentum scale $\overline{\Lambda}_\chi$, at which the theory breaks down because new degrees of freedom enter[3]. While $\frac{m_\pi}{\overline{\Lambda}_\chi}$ and $\frac{\Delta_M}{\overline{\Lambda}_\chi}$ have quite different chiral behaviour, we follow Pascalutsa and Phillips [29] and take a common breakdown scale $\overline{\Lambda}_\chi \approx 650$ MeV, consistent with the masses of the ω and ρ as the next-lightest exchange mesons, exploiting a numerical coincidence at the physical pion mass to define a single expansion parameter:

$$\delta \equiv \frac{\Delta_M}{\overline{\Lambda}_\chi} \approx \sqrt{\frac{m_\pi}{\overline{\Lambda}_\chi}} \approx \sqrt{\frac{\omega}{\overline{\Lambda}_\chi}} \approx 0.4 \ll 1 \quad . \tag{3.5}$$

[3]This physically meaningful parameter is not to be confused with an unphysical "cutoff" Λ, albeit the symbols are similar [28, 27].

We also count $M_{\rm N} \sim \overline{\Lambda}_\chi$. Since δ is not very small, order-by-order convergence must be verified carefully, see sect. refsec:uncertainties.

This power counting organises contributions under the assumption $\omega \sim m_\pi$. As extensively discussed previously [31, 30, 33, 32, 34] and summarised in [36, sect. 5.2], in this régime only kernels with one and two active nucleons contribute in a χEFT description of Compton scattering up to and including N^{4}LO [$\mathcal{O}(e^2\delta^4)$]. At lower energies $\omega \lesssim m_\pi^2/M$, this power counting does not apply because photons with resolution $1/\omega$ larger than the size of the ^{4}He nucleus scatter coherently on the whole target. Refs. [33, 32, 36] discuss in detail how the reformulated power counting appropriate at these lower energies leads to the restoration of the Thomson limit by inclusion of coherent propagation of the ^{4}He system in the intermediate state between absorption and emission of photons. This rescattering effect involves the interaction of all A nucleons with one another between photon absorption and emission, and hence an A-body density. However, that régime is not the focus of this presentation. Rather, we are concerned with the non-collective contributions which dominate above about 50 MeV. That is also where data is most likely to be taken to extract nucleon polarisabilities.

Specifically, we use the one- and two-body Compton kernels of refs. [26, 25, 31], supplemented with the Δ-pole and $\pi\Delta$ loop graphs [23, 24, 33, 32]. They are both conceptually and numerically identical to the ones which have been described extensively in our Compton studies of the deuteron [33, 32, 22, 21, 20] and, most recently, ^{3}He [34, 44]. These pieces of the photonuclear operator are organised in a perturbative expansion which is complete up to and including N^{3}LO [$\mathcal{O}(e^2\delta^3)$]. No contribution enters at NLO [$\mathcal{O}(e^2\delta^1)$], and only one-body Delta contributions at N^{3}LO [$\mathcal{O}(e^2\delta^3)$]. We only allow photon energies somewhat below $\omega_{\rm thr}(^4{\rm He}) \approx m_\pi$ in order to avoid additional complications in the vicinity of the pion-production threshold.

The one-nucleon kernel convoluted with the one-body density as in eq. (2.3).

(a) LO [$\mathcal{O}(e^2\delta^0 = Q^2)$]: The single-nucleon (proton) Thomson term.

(b) N^{2}LO [$\mathcal{O}(e^2\delta^2 = Q^3)$] non-structure/Born terms: photon couplings to the nucleon charge beyond LO, to its magnetic moment, or to the t-channel exchange of a π^0 meson (irrelevant for the isoscalar ^{4}He).

(c) N^{2}LO [$\mathcal{O}(e^2\delta^2 = Q^3)$] structure/non-Born terms: photon couplings to the pion cloud around the nucleon is the source of the LO contributions to the polarisabilities as first reported in refs. [26, 25].

(d/e) N^{3}LO [$\mathcal{O}(e^2\delta^3)$] structure/non-Born terms: photon couplings to the pion cloud around the (non-relativistic) $\Delta(1232)$ (d) or directly exciting the Delta (e), as calculated in refs. [18, 19, 15]; these give NLO contributions to the polarisabilities. The Delta parameters are taken from ref. [34]. The Delta excitation of diagram (d) shows considerable energy dependence even at $\omega \sim m_\pi$; see the discussion of "dynamical polarisabilities" in refs. [36, 16]. This will be important in the interpretation of our results in sect. Results.

(f) Short-distance/low-energy coefficients (LECs) encode those contributions to the nucleon polarisabilities which stem from physics at and above the breakdown

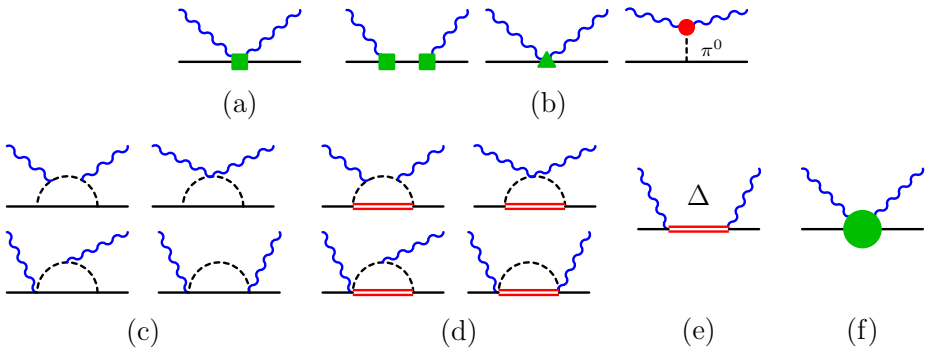

Figure 4: (Colour on-line) The single-nucleon contributions in χEFT up to N^{3}LO [$\mathcal{O}(e^2\delta^3)$] for 50 MeV $\lesssim \omega \lesssim$ 120 MeV. The vertices are from: $\mathcal{L}^{(1)}_{\pi N}$ (no symbol), $\mathcal{L}^{(2)}_{\pi N}$ (green square), $\mathcal{L}^{(3)}_{\pi N}$ (green triangle), $\mathcal{L}^{(4)}_{\pi\pi}$ (red disc) [25]; the green disc of graph (f) stands for variations of the polarisabilities. Permuted and crossed diagrams are not displayed.

scale $\overline{\Lambda}_\chi$. These offsets to the polarisabilities are formally of higher order. We determine them to reproduce the isoscalar polarisabilities of eq. (1.2). Their uncertainties were discussed in the Introduction but are dwarfed by the other uncertainties of the results presented here, including those coming from the wave function dependence and higher order effects; see sect. 4.3. Neither does the detailed discussion of the sources and sizes of uncertainties of other nucleon polarisabilities in ref. [38] bear on the present results. We also recall from the Introduction that since ^{4}He is a near-perfect isoscalar and scalar, neither the nucleon's isovector polarisabilities nor its spin polarisabilities enter, except at very high orders.

The first nonzero two-body kernel convoluted with the two-body density as in eq. (2.4) enters at N^{2}LO [$\mathcal{O}(e^2\delta^2)$] and does not involve Delta excitations; see fig. 5. It is the two-body analogue of the πN loop graphs (c) in fig. 4, first computed for $t_{12} = 0$ in refs. [31, 30] and extended to $t_{12} = 1$ in refs. [17, 14, 13] where full expressions can be found. These contributions are nonzero only for np pairs, that is, they all contain the same 2N isospin factor.

$$\langle t_{12} m^{t\prime}_{12} | (\tau^{(1)} \cdot \tau^{(2)} - \tau^{(1)}_z \tau^{(2)}_z) | t_{12} m^t_{12} \rangle = 2(-1)^{t_{12}+1}\, \delta_{m^{t\prime}_{12} m^t_{12}}\, \delta_{m^t_{12} 0} \quad . \tag{3.6}$$

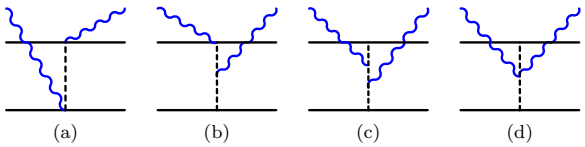

Figure 5: (Colour on-line) N^{2}LO [$\mathcal{O}(e^2\delta^2)$] contributions to the (irreducible) γNN $\to$ γNN amplitude (no additional contributions at N^{3}LO [$\mathcal{O}(e^2\delta^3)$]. Notation as in fig. 4. Permuted and crossed diagrams not displayed.

Therefore, they parametrise the leading term of both photons hitting the charged-meson-exchange. In ^{4}He, as in ^{3}He, both isospin $t_{12} = 0$ and 1 pairs are present. Corrections to these currents enter at one order higher, N^{4}LO [$\mathcal{O}(e^2\delta^4)$], than we consider here.

3.3 Creation of Transition Probability Densities from Chiral Potentials

Again this is taken directly from the ^{4}He paper

We used a class of four chiral 2N and 3N interactions to generate the one- and two-body densities for ^{4}He: the χEFT Semi-local Momentum-Space (SMS) 2N potentials in the version "N^{4}LO +" (*i.e.* considered to be complete at N^{4}LO with some N^{5}LO interactions) [8] and the corresponding chiral 3N interaction "N^{2}LO" discussed in ref. [12]. We employed 2N momentum-space cutoffs $\Lambda = 550$ MeV (hardest), 500 MeV, 450 MeV and 400 MeV (softest) (the complete set of parameters of the 3N interactions can be found in Table 1 of Ref. [11]). These nuclear interactions all capture the correct long-distance physics of one- and two-pion exchange and reproduce both the 2N scattering data and the experimental values of the triton and ^{3}He binding energies well. Increasing momentum cutoffs indicate increasing "hardness" of the short-distance interaction. Their ^{4}He binding energies are within +0.5 MeV ($\Lambda = 550$ MeV) to −0.1 MeV ($\Lambda = 400$ MeV) of the experimental value. This variation by less than 2% is not a concern, since we compute for photon energies that are high enough that this slight variation in the ^{4}He binding energy has no impact on the elastic Compton cross section.

These are of course but four out of a number of modern, sophisticated potentials. Our choice is dictated by the fact that they are semi-local (and hence of the form of AV18) and are already coded for the densities formalism. By varying the cutoff within a single family of χEFT potentials, we avoid questions about how the cutoffs of different realisations of the χEFT regulator functions are related. The range of cutoffs chosen, while not large enough to establish renormalisability of the theory, is large enough to indicate a lower bound of the sensitivity of cross sections to the short-distance physics of this process.

These χEFT wave functions use Weinberg's "hybrid approach" [10], in which potentials are derived to an assumed accuracy and then iterated to produce amplitudes or, in our case, one- and two-body densities. All claim a higher accuracy than that of our Compton kernels. We refrain here from entering the ongoing debate about correct implementations of the chiral power counting or the range of cutoff variations, etc.; see refs. [9, 7] for concise summaries, ref. [27] for a polemic, and ref. [6] for a variety of community voices.

Similarly, even though the Compton Ward identities are violated because the one-pion-exchange 2N potentials are regulated, any inconsistencies between currents and nuclear densities is compensated by operators which enter at higher orders in χEFT than the last order we fully retain [N^{3}LO, $\mathcal{O}(e^2\delta^3)$]. In addition, the potentials do not include explicit Delta contributions while the kernel does. However, it is easy

to see that, for real Compton scattering around 120 MeV, a Delta excited directly by the incoming photon is more important than one that occurs virtually between exchanges of virtual pions, especially for an isoscalar target like ^{4}He. For our purposes, such Delta excitations in the 2N potential are already suppressed by several orders in the chiral counting and well approximated by the πN seagull Low Energy Coefficients that enter the N^{3}LO interaction.

sect. **??**, we therefore take the differences between results with the 4 fferent sets of densities as providing a lower bound indicative of the esent residual theoretical uncertainties. These do not affect the nclusions of our sensitivity studies, but better extractions of larisabilities from ^{4}He data will undoubtedly need a reduced potential spread. The results generated with the potential χSMSN^{4}LO+450MeV+N^{2}LO3NI turn out to be approximately the mean of those generated from the different potentials considered, so we use that for central values, and assess variations with respect to it.

The ^{4}He one- and two-body densities, together with the ^{3}He densities, are publicly available using the python package provided at `https://pypi.org/project/nucdens/`. They are defined in momentum space, for centre-of-mass energies and momentum transfers corresponding to Compton scattering photon energies between $\omega_{\rm cm} = 50$ and 120 MeV in steps of 10 MeV and scattering angles $\theta_{\rm cm} \in [0; 180°]$ in steps of 15° (momentum-transfers $\sqrt{\vec{q}^2} \in [0; 240]$ MeV), plus at selected higher and lower energies for control. Also available are densities using the harder AV18 2N model interaction [5], supplemented by the Urbana-IX 3N interaction (3NI) [4, 3], and densities using the chiral Idaho interaction for the 2N system in the version "N^{3}LO" at cutoff 500 MeV [2] with the χEFT 3N interaction in the version "$\mathcal{O}(Q^3)$" using variant "b" of ref. [1] as the "softest" choice.

4 Results

4.1 Differential Cross Section

Differential cross section plot here

4.2 Comparison to Experimental Data

Gerry's data goes here

4.3 Uncertainty Analysis

Bayesian approach blah blah blah

4.3.1 A-Priori estimate

What is this?

4.3.2 Convergence of the Chiral EFT Expansion

Show convergence order by order

4.3.3 SRG Induced Many-Body Forces

Compare to ^{4}He maybe?

4.3.4 Residual Dependence on the 2N and 3N Interactions

4.3.5 Numerical Uncertainty

4.3.6 Total Uncertainty

Plot about dependence on α_{E1}, β_{M1}

4.4 Sensitivity to the Scalar-Isoscalar Polarisabilities

4.5 Beam Asymmetry

Plots here

4.6 Comparison with Other Few Nucleon Targets

Plot of ratios here

5 Summary and Conclusions

References

[1] A. Nogga, P. Navrátil, B. R. Barrett, and J. P. Vary, "Spectra and binding energy predictions of chiral interactions for ^{7}Li,"
Physical Review C **73** (2006) 064002.
DOI: 10.1103/PhysRevC.73.064002.

[2] D. R. Entem and R. Machleidt, "Accurate charge-dependent nucleon-nucleon potential at fourth order of chiral perturbation theory,"
Physical Review C **68** (2003) 041001.
DOI: 10.1103/PhysRevC.68.041001.

[3] B. S. Pudliner, V. R. Pandharipande, J. Carlson, S. C. Pieper, and R. B. Wiringa, "Quantum Monte Carlo calculations of nuclei with $A \leq 7$,"
Physical Review C **56** (1997) 1720–1750.
DOI: 10.1103/PhysRevC.56.1720.

[4] B. S. Pudliner, V. R. Pandharipande, J. Carlson, and R. B. Wiringa, "Quantum Monte Carlo Calculations of $A \leq 6$ Nuclei,"
Physical Review Letters **74** (1995) 4396–4399.
DOI: 10.1103/physrevlett.74.4396.

[5] R. B. Wiringa, V. G. J. Stoks, and R. Schiavilla, "Accurate nucleon-nucleon potential with charge-independence breaking,"
Physical Review C **51** (1995) 38–51.
DOI: 10.1103/physrevc.51.38.

[6] Ingo Tews *et al.*, "Nuclear Forces for Precision Nuclear Physics: A Collection of Perspectives,"
Few-Body Systems **63** (2022).
DOI: 10.1007/s00601-022-01749-x.

[7] U. van Kolck, "The Problem of Renormalization of Chiral Nuclear Forces,"
arXiv:2003.06721 (2020). Available at: `https://arxiv.org/abs/2003.06721`.

[8] P. Reinert, H. Krebs, and E. Epelbaum, "Semilocal momentum-space regularized chiral two-nucleon potentials up to fifth order,"
The European Physical Journal A **54** (2018) Article 12516.
DOI: 10.1140/epja/i2018-12516-4.

[9] D. R. Phillips, "Recent results in chiral effective field theory for the NN system,"
arXiv:1302.5959 (2013). Available at: `https://arxiv.org/abs/1302.5959`.

[10] S. Weinberg, "Nuclear forces from chiral lagrangians,"
Physics Letters B **251** (1990) 288–292.
DOI: 10.1016/0370-2693(90)90938-3.

[11] H. Le, J. Haidenbauer, U. G. Meißner, and A. Nogga, "Separation energies of light Λ hypernuclei and their theoretical uncertainties,"
arXiv:2308.01756, DOI: 10.1140/epja/s10050-023-01219-w.

[12] P. Maris *et al.* (Lenpic Collaboration), "Light nuclei with semilocal momentum-space regularized chiral interactions up to third order,"
Physical Review C **103** (2021) 054001.
DOI: 10.1103/PhysRevC.103.054001.

[13] D. Shukla, "Investigating Neutron Polarizabilities and NN Scattering in Heavy-Baryon Chiral Perturbation Theory,"
Ph.D. thesis. Available at: `http://rave.ohiolink.edu/etdc/view?acc_num=ohiou1163711618`.

[14] D. Shukla, A. Nogga, and D. R. Phillips, "Analyzing the effects of neutron polarizabilities in elastic Compton scattering off ^{3}He,"
Nuclear Physics A **819** (2009) 98–134.
DOI: 10.1016/j.nuclphysa.2009.01.003.

[15] T. R. Hemmert, B. R. Holstein, J. Kambor, and G. Knöchlein, "Compton scattering and the spin structure of the nucleon at low energies,"
Physical Review D **57** (1998) 5746–5754.
DOI: 10.1103/physrevd.57.5746.

[16] H. W. Grießhammer, J. A. McGovern, and D. R. Phillips, "Comprehensive study of observables in Compton scattering on the nucleon,"
The European Physical Journal A **54** (2018) Article 12467.
DOI: 10.1140/epja/i2018-12467-8.

[17] D. Choudhury, A. Nogga, and D. R. Phillips, "Investigating Neutron Polarizabilities through Compton Scattering on ^{3}He,"
Physical Review Letters **98** (2007) 232303.
DOI: 10.1103/physrevlett.98.232303.

[18] M. N. Butler and M. J. Savage, "Electromagnetic polarisability of the nucleon in chiral perturbation theory,"
Physics Letters B **294** (1992) 369–374.
DOI: 10.1016/0370-2693(92)91535-h.

[19] T. R. Hemmert, B. R. Holstein, and J. Kambor, "Delta(1232) and the Polarizabilities of the Nucleon,"
Physical Review D **55** (1997) 5598–5612.
DOI: 10.1103/physrevd.55.5598.

[20] L. S. Myers *et al.*, "Compton scattering from the deuteron below pion-production threshold,"
Physical Review C **92** (2015) 025203.
DOI: 10.1103/physrevc.92.025203.

[21] L. S. Myers *et al.*, "Measurement of Compton Scattering from the Deuteron and an Improved Extraction of the Neutron Electromagnetic Polarizabilities,"
Physical Review Letters **113** (2014) 262506.
DOI: 10.1103/physrevlett.113.262506.

[22] H. W. Grießhammer, "Dissecting deuteron Compton scattering I: The observables with polarised initial states,"
European Physical Journal A.
DOI: 10.1140/epja/i2013-13100-2. (Note: Detailed volume and year information was not provided in the original entry.)

[23] R. P. Hildebrandt, H. W. Grießhammer, T. R. Hemmert, and B. Pasquini, "Signatures of chiral dynamics in low-energy Compton scattering off the nucleon,"
The European Physical Journal A **20** (2004) 293–315.
DOI: 10.1140/epja/i2003-10144-9.

[24] R. P. Hildebrandt, H. W. Grießhammer, T. R. Hemmert, and D. R. Phillips, "Explicit $\Delta(1232)$ degrees of freedom in Compton scattering off the deuteron,"

Nuclear Physics A **748** (2005) 573–595.
DOI: 10.1016/j.nuclphysa.2004.11.017.

[25] V. Bernard, N. Kaiser, and Ulf-G. Meißner, "Chiral dynamics in nucleons and nuclei,"
International Journal of Modern Physics E **4**, no. 2 (1995) 193–344.
DOI: 10.1142/s0218301395000092.

[26] V. Bernard, N. Kaiser, and Ulf-G. Meißner, "Chiral expansion of the nucleon's electromagnetic polarizabilities,"
Physical Review Letters **67** (1991) 1515–1518.
DOI: 10.1103/PhysRevLett.67.1515.

[27] H. W. Grießhammer, "What Can Possibly Go Wrong?,"
Few-Body Systems **63** (2022) Article 01739-z.
DOI: 10.1007/s00601-022-01739-z.

[28] R. J. Furnstahl, D. R. Phillips, and S. Wesolowski, "A recipe for EFT uncertainty quantification in nuclear physics,"
Journal of Physics G: Nuclear and Particle Physics **42** (2015) 034028.
DOI: 10.1088/0954-3899/42/3/034028.

[29] V. Pascalutsa and D. R. Phillips, "Effective theory of the Delta(1232) resonance in Compton scattering off the nucleon,"
Physical Review C **67** (2003) 055202.
DOI: 10.1103/physrevc.67.055202.

[30] S. R. Beane, M. Malheiro, J. A. McGovern, D. R. Phillips, and U. van Kolck, "Compton scattering on the proton, neutron, and deuteron in chiral perturbation theory,"
Nuclear Physics A **747** (2005) 311–361.
DOI: 10.1016/j.nuclphysa.2004.09.068.

[31] S. R. Beane, M. Malheiro, D. R. Phillips, and U. van Kolck, "Compton scattering on the deuteron in baryon chiral perturbation theory,"
Nuclear Physics A **656** (1999) 367–399.
DOI: 10.1016/s0375-9474(99)00312-7.

[32] R. P. Hildebrandt, H. W. Grießhammer, and T. R. Hemmert, "Nucleon polarizabilities from deuteron Compton scattering within a Green's function hybrid approach,"
The European Physical Journal A **46** (2010) 111–137.
DOI: 10.1140/epja/i2010-11024-y.

[33] R. P. Hildebrandt, "Elastic Compton Scattering from the Nucleon and Deuteron,"
arXiv:nucl-th/0512064 (2005). Available at: `https://arxiv.org/abs/nucl-th/0512064`.

[34] A. Margaryan, B. Strandberg, H. W. Grießhammer, J. A. McGovern, D. R. Phillips, and D. Shukla, "Elastic Compton scattering from ^{3}He and the role of the Delta,"
The European Physical Journal A **54** (2018) Article 12554.
DOI: 10.1140/epja/i2018-12554-x.

[35] J. A. McGovern, D. R. Phillips, and H. W. Grießhammer, "Compton scattering from the proton in an effective field theory with explicit Delta degrees of freedom,"
The European Physical Journal A **49** (2013) 13012–1.
DOI: 10.1140/epja/i2013-13012-1.

[36] H. W. Grießhammer, J. A. McGovern, D. R. Phillips, and G. Feldman, "Using Effective Field Theory to analyse low-energy Compton scattering data from protons and light nuclei,"
Progress in Particle and Nuclear Physics **67** (2012) 841–897.
DOI: 10.1016/j.ppnp.2012.04.003.

[37] J. de Vries, C. Köber, A. Nogga, and S. Shain, "Dark matter scattering off ^{4}He in chiral effective field theory,"
arXiv:2310.11343 (2023). Available at: `https://arxiv.org/abs/2310.11343`.

[38] H. W. Grießhammer, J. A. McGovern, and D. R. Phillips, "Nucleon polarisabilities at and beyond physical pion masses,"
The European Physical Journal A **52** (2016) Article 16139–5.
DOI: 10.1140/epja/i2016-16139-5.

[39] L. S. Myers *et al.*, "Compton scattering from the deuteron below pion-production threshold,"
Physical Review C **92** (2015) 025203.
DOI: 10.1103/physrevc.92.025203.

[40] L. S. Myers *et al.*, "Measurement of Compton Scattering from the Deuteron and an Improved Extraction of the Neutron Electromagnetic Polarizabilities,"
Physical Review Letters **113** (2014) 262506.
DOI: 10.1103/physrevlett.113.262506.

[41] H. W. Grießhammer, J. Liao, J. A. McGovern, A. Nogga, and D. R. Phillips, "Compton Scattering on ^{4}He with Nuclear One- and Two-Body Densities,"
arXiv:2401.16995 (2024). Available at: `https://arxiv.org/abs/2401.16995`.

[42] L. S. Myers, M. W. Ahmed, G. Feldman, S. S. Henshaw, M. A. Kovash, J. M. Mueller, and H. R. Weller, "Compton scattering from Li-6 at 60 MeV,"
Physical Review C **86** (2012) 044614.
DOI: 10.1103/PhysRevC.86.044614.

[43] L. S. Myers, M. W. Ahmed, G. Feldman, A. Kafkarkou, D. P. Kendellen, I. Mazumdar, J. M. Mueller, M. H. Sikora, H. R. Weller, and W. R. Zimmerman,

"Compton Scattering from ^{6}Li at 86 MeV,"
Physical Review C **90** (2014) 027603.
DOI: 10.1103/PhysRevC.90.027603.

[44] H. W. Grießhammer, J. A. McGovern, A. Nogga, and D. R. Phillips, "Scattering Observables from One- and Two-body Densities: Formalism and Application to ^{3}He Scattering,"
Few-Body Systems **61** (2020) Article 01578–w.
DOI: 10.1007/s00601-020-01578-w.

[45] S. Szpigel and R. J. Perry, "The Similarity Renormalization Group,", Quantum Field Theory: A Twentieth Century Profile,

[46] R. J. Furnstahl and K. Hebeler, "New applications of renormalization group methods in nuclear physics," *Reports on Progress in Physics*, vol. 76, no. 12, p. 126301, Nov. 2013. DOI: 10.1088/0034-4885/76/12/126301.

[47] X.-X. Sun, H. Le, A. Nogga, and U.-G. Meißner, in preparation (2025).

[48] P. Reinert, H. Krebs, and E. Epelbaum, "Semilocal momentum-space regularized chiral two-nucleon potentials up to fifth order," *The European Physical Journal A*, vol. 54, no. 5, May 2018. DOI: 10.1140/epja/i2018-12516-4.